

Drag force of Anisotropic plasma at finite $U(1)$ chemical potential

Long Cheng¹, Xian-Hui Ge¹, Shang-Yu Wu^{2,3}

¹*Department of Physics, Shanghai University, Shanghai 200444, China*

²*Department of Electrophysics, and Yau Shing Tung Center, National Chiao Tung University, Hsinchu 300, Taiwan.*

³*National Center for Theoretical Science, Hsinchu, Taiwan.*

physcheng@shu.edu.cn, gexh@shu.edu.cn, loganwu@gmail.com

Abstract

We perform the calculation of drag force acting on a massive quark moving through an anisotropic $\mathcal{N} = 4$ SU(N) Super Yang-Mills plasma in the presence of a $U(1)$ chemical potential. We present the numerical results for any real (prolate solution) or imaginary (oblate solution) value of anisotropy and arbitrary direction of the quark velocity with respect to the direction of anisotropy. We find the effect of chemical potential or charge density will enhance the drag force for the prolate solution, and opposite to the oblate solution. On the other hand, as the anisotropy increases, the drag force is enhanced, and the effect of chemical potential strengthens the enhancement.

1 Introduction

The experiments data in the Relativistic Heavy Ion Collider (RHIC) [1, 2] show that the quark gluon plasma (QGP), as deconfined phase of QCD at high temperature and high charge density, is the strongly coupled fluid rather than the weakly coupled gas of quarks and gluons. Thus the perturbative QCD is no longer reliable and we should explore the non-perturbative calculational methods of QCD.

The AdS/CFT correspondence [3–5] provides a powerful tool to investigate various strongly coupled systems in condensed matter physics (for reviews, see[6, 7]) like superconductors [8–10], Lifshitz fixed point [11–14], Quantum chromodynamics [15, 16] and heavy ion collisions like photon production [17, 18], elliptic flow [19], drag force [21, 22], jet quenching [23, 24] and anomalous transport [25–28]. Using the AdS/CFT correspondence, we can study the strongly $\mathcal{N} = 4$ Super-Yang-Mills plasma through considering IIB supergravity in $AdS_5 \times S^5$. One significant result is the calculation of the ratio of shear viscosity to entropy density of QGP, this ratio is universal and equal to $1/4\pi$ [20], which matches the experiment data very well. So the AdS/CFT give a reliable way to investigate the quantities of QGP.

It is well-known that the most important quantities of QGP are drag force and jet-quenching parameter. In the context of AdS/CFT [21, 22], the moving heavy quark in the thermal medium is dual to a probe open string with infinite mass, which is attached to the boundary of bulk space-time and stretch to the black hole horizon. So the dynamics of string can give us the effects of $\mathcal{N} = 4$ Super-Yang-Mills plasma in which quark is moving. The similar study for jet quenching for $\mathcal{N} = 4$ SYM plasma can be found in [23, 24], where the jet-quenching parameter was obtained by calculating the expectation value of a closed light-like Wilson loop in the dipole approximation.

In this paper, we will study the moving quark in the anisotropic QGP with chemical potential, since the QGP after creation in a short time is anisotropic and real experiments are done at finite baryon chemical potential. From the point of view of holography, the anisotropic plasma with chemical potential is dual to a anisotropic charged black brane [29, 30], hence to compute the drag force experienced by an infinitely massive quark, we should consider a string in anisotropic charged black brane. We will show the results analytically and numerically respectively. The discussion for chargeless anisotropic plasma and its energy loss in the framework of AdS/CFT can be found in [18, 31–35].

This paper is organized as follows. In Section 2, we briefly describe the construction of

the anisotropic charged black brane solution. In Section 3, we calculate the drag force acting on a massive quark moving through the plasma. Furthermore, in the small anisotropy and high temperature limit, we can perform the calculation of the drag force analytically. In Section 4, we show our numerical results for the prolate and oblate anisotropy, respectively. In Section 5, we conclude with a brief summary of our results.

Note: When this paper is in the preparation, the paper [37] appeared which has some overlap with this paper. The differences between our paper and [37], are that we consider the drag force for the oblate anisotropy with $a^2 < 0$ and the large charge case in particular.

2 Anisotropic charged black brane solution

The AdS_5 part of ten dimensional anisotropic IIB supergravity solution in Einstein frame is given by [30],

$$ds^2 = \frac{e^{-\frac{1}{2}\phi}}{u^2} \left(-\mathcal{F}\mathcal{B} dt^2 + dx^2 + dy^2 + \mathcal{H}dz^2 + \frac{du^2}{\mathcal{F}} \right), \quad (1)$$

$$A = A_t(u)dt, \quad \text{and} \quad \chi = az, \quad (2)$$

which was obtained by dimensional reduction on S^5 from the ten-dimensional metric. So we have ignored the metric of the S^5 part that will play no role in the following discussions and our treatment is in agreement with ten dimensional framework.

The spacetime is required to be anisotropic but homogenous, so that the functions ϕ , \mathcal{F} , \mathcal{B} and $\mathcal{H} = e^{-\phi}$ should only depend on the radial coordinate u . The electric potential A_t in this metric is expressed as $A_t(u) = -\int_{u_H}^u du Q \sqrt{\mathcal{B}} e^{\frac{3}{4}\phi} u$ from the Maxwell equations, where Q is an integral constant related to the charge density. Note that the electric potential has a contribution from the anisotropy through the dilatonic field ϕ . The horizon and boundary are at $u = u_H$ and $u = 0$ respectively. The asymptotic AdS boundary requires $\mathcal{F} = \mathcal{B} = \mathcal{H} = 1$. We can plot the numerical solutions [30] in Figs.1 for both $a^2 > 0$ and $a^2 < 0$ cases. We mean prolate and oblate anisotropy, since $\mathcal{H}(u_H) > 1$ for the $a^2 > 0$ case and $\mathcal{H}(u_H) < 1$ for the $a^2 < 0$ case.

In the small anisotropy and charge limits, we can obtain the high temperature solution,

$$\begin{aligned} \mathcal{F} &= 1 - \left(\frac{u}{u_H}\right)^4 + \left[\left(\frac{u}{u_H}\right)^6 - \left(\frac{u}{u_H}\right)^4 \right] q^2 + a^2 \mathcal{F}_2(u) + \mathcal{O}(a^4), \\ \mathcal{B} &= 1 + a^2 \mathcal{B}_2(u) + \mathcal{O}(a^4), \\ \mathcal{H} &= e^{-\phi(u)}, \quad \text{with} \quad \phi(u) = a^2 \phi_2(u) + \mathcal{O}(a^4), \end{aligned} \quad (3)$$

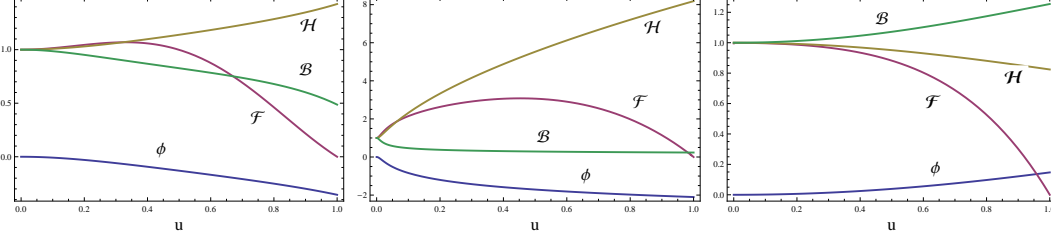


Figure 1: (Color online.) The metric functions for $a = 1.86$, $Q = 6.23$ (left), $a = 64.06$, $Q = 9.76$ (middle) and $a = 1.2i$, $Q = 1/10$ (right), with $u_H = 1$.

where $\mathcal{F}_2(u) = \hat{\mathcal{F}}_0(u) + \hat{\mathcal{F}}_2(u)q^2 + O(q^4)$, $\mathcal{B}_2(u) = \hat{\mathcal{B}}_0(u) + \hat{\mathcal{B}}_2(u)q^2 + O(q^4)$ and $\phi_2(u) = \hat{\phi}_0(u) + \hat{\phi}_2(u)q^2 + O(q^4)$ with

$$\begin{aligned}
\hat{\mathcal{F}}_0(u) &= \frac{1}{24u_H^2} \left[8u^2(u_H^2 - u^2) - 10u^4 \log 2 + (3u_H^4 + 7u^4) \log \left(1 + \frac{u^2}{u_H^2} \right) \right], \\
\hat{\mathcal{B}}_0(u) &= -\frac{u_H^2}{24} \left[\frac{10u^2}{u_H^2 + u^2} + \log \left(1 + \frac{u^2}{u_H^2} \right) \right], \\
\hat{\phi}_0(u) &= -\frac{u_H^2}{4} \log \left(1 + \frac{u^2}{u_H^2} \right).
\end{aligned} \tag{4}$$

and

$$\begin{aligned}
\hat{\mathcal{F}}_2(u) &= \frac{1}{24u_H^4(u^2 + u_H^2)} \left[7u^8 + 6u^2u_H^6 + u^4u_H^4(25 \log 2 - 12), \right. \\
&\quad \left. + u^6u_H^2(25 \log 2 - 1) - (u^2 + u_H^2)(12u^6 + 7u^4u_H^2 + 6u_H^6) \log \left(1 + \frac{u^2}{u_H^2} \right) \right], \\
\hat{\mathcal{B}}_2(u) &= \frac{1}{24} \left[-\frac{u^2(11u^4 + 3u^2u_H^2 + 2u_H^4)}{(u^2 + u_H^2)^2} + 2u_H^2 \log \left(1 + \frac{u^2}{u_H^2} \right) \right], \\
\hat{\phi}_2(u) &= \frac{1}{4} \left[-2u^2 + \frac{u^4}{u^2 + u_H^2} + 2u_H^2 \log \left(1 + \frac{u^2}{u_H^2} \right) \right].
\end{aligned} \tag{5}$$

where we have used the dimensionless parameter $q = \frac{u_H^3 Q}{2\sqrt{3}}$. Here we would like to justify the usage of the the small anisotropy and charge limits. The analytic solution for the non-perturbative charge was given in [29, 30]. Unfortunately, for the analytic computation of the drag force, it is too difficult to determine some critical parameters.

Having the metric of the black brane, we can easily obtain the temperature as

$$T = -\frac{\mathcal{F}'(u_H)\sqrt{\mathcal{B}(u_H)}}{4\pi}. \tag{6}$$

Note that the temperature can not be zero unless $a^2 \leq 0$ which corresponds to the "oblate" case, by contrast, $a^2 > 0$ corresponds to "prolate" case.

3 Drag force

On the anisotropic charged brane background, the Nambu-Goto action which governs the dynamics of a probe string is

$$S = -T_0 \int d^2\sigma e^{\phi/2} \sqrt{-\det g_{\alpha\beta}} \quad (7)$$

where $T_0 = \frac{1}{2\pi\alpha'}$ is the string tension and $g_{\alpha\beta} \equiv G_{\mu\nu}\partial_\alpha X^\mu\partial_\beta X^\nu$ is induced metric on the two-dimensional worldsheet. $X^\mu(\sigma^\alpha)$ are the embedding equations of worldsheet in spacetime. In what follows, we will work in the static gauge, i.e. $\sigma = u$ and $\tau = t$. Since the plasma is anisotropic, we consider the motions of the string in two different directions x and z , which is corresponding to the quark moving at constant velocity v . It is convenient to set the configuration of string as [33]

$$\begin{aligned} x(u, t) &= x(u) \sin \theta + vt \sin \theta \\ z(u, t) &= z(u) \cos \theta + vt \cos \theta. \end{aligned} \quad (8)$$

Obviously θ is the angle between z-axis and velocity.

The determinant of $g_{\alpha\beta}$ satisfies

$$-ge^{\phi} = \frac{-v^2 (\sin^2 \theta + (1 + \mathcal{F} \sin^2 \theta (x' - z')^2) \mathcal{H} \cos^2 \theta) + \mathcal{B}\mathcal{F} (1 + \mathcal{F} (x'^2 \sin^2 \theta + \mathcal{H} z'^2 \cos^2 \theta))}{u^4 \mathcal{F}}, \quad (9)$$

so the Lagrangian $\mathcal{L} = -T_0 e^{\phi/2} \sqrt{-g}$ gives the canonical momenta density to the string as

$$\begin{aligned} \Pi_x^\sigma &= \frac{\partial \mathcal{L}}{\partial x'} = -T_0 e^{-\phi/2} \frac{x' \mathcal{B}\mathcal{F} + v^2 \mathcal{H} (z' - x') \cos^2 \theta}{u^4 \sqrt{-g}} \sin \theta \\ \Pi_z^\sigma &= \frac{\partial \mathcal{L}}{\partial z'} = -T_0 e^{-\phi/2} \frac{z' \mathcal{B}\mathcal{F} + v^2 \mathcal{H} (x' - z') \sin^2 \theta}{u^4 \sqrt{-g}} \cos \theta, \end{aligned} \quad (10)$$

where the prime denotes the derivative with respect to u . Then the equations of motion following from Nambu-Goto action are

$$\begin{aligned} \partial_u \left(-T_0 e^{-\phi/2} \frac{x' \mathcal{B}\mathcal{F} + v^2 \mathcal{H} (z' - x') \cos^2 \theta}{u^4 \sqrt{-g}} \sin \theta \right) &= 0 \\ \partial_u \left(-T_0 e^{-\phi/2} \frac{z' \mathcal{B}\mathcal{F} + v^2 \mathcal{H} (x' - z') \sin^2 \theta}{u^4 \sqrt{-g}} \cos \theta \right) &= 0. \end{aligned} \quad (11)$$

Note that in string configuration (8), the time part of E.O.M is vanish because of time independence. Then after integration of (11), we have

$$\begin{aligned} -T_0 e^{-\phi/2} \frac{x' \mathcal{B}\mathcal{F} + v^2 \mathcal{H} (z' - x') \cos^2 \theta}{u^4 \sqrt{-g}} \sin \theta &= C, \\ -T_0 e^{-\phi/2} \frac{z' \mathcal{B}\mathcal{F} + v^2 \mathcal{H} (x' - z') \sin^2 \theta}{u^4 \sqrt{-g}} \cos \theta &= D, \end{aligned} \quad (12)$$

which involve

$$\begin{aligned} x' &= \frac{e^{\phi/2} u^4 \csc \theta \sqrt{-g} (v^2 (C + D \cot \theta) - C \mathcal{B} \mathcal{F} \csc^2 \theta)}{T_0 \mathcal{B} \mathcal{F} (\mathcal{B} \mathcal{F} \csc^2 \theta - v^2 (1 + \mathcal{H} \cot^2 \theta))}, \\ z' &= \frac{e^{\phi/2} u^4 \csc \theta \sqrt{-g} \sec \theta (v^2 \mathcal{H} (D \csc \theta + C \sec \theta) - D \mathcal{B} \mathcal{F} \csc \theta \sec^2 \theta)}{T_0 \mathcal{B} \mathcal{F} \mathcal{H} (4 \mathcal{B} \mathcal{F} \csc^2 2\theta - v^2 (\mathcal{H} \csc^2 \theta + \sec^2 \theta))}, \end{aligned} \quad (13)$$

where the constant C and D are integral constants corresponding to momenta in two directions. Taking (13) back to (9), we can solve the determinant of induced metric as

$$-ge^\phi = -\frac{2T_0 \mathcal{B} \mathcal{H} (\mathcal{B} \mathcal{F} - v^2 (\cos^2 \theta \mathcal{H} + \sin^2 \theta))^2}{I(u)}, \quad (14)$$

with

$$\begin{aligned} I(u) &= u^4 \left[-2T_0^2 \mathcal{B}^2 \mathcal{F}^2 \mathcal{H} + \mathcal{B} \mathcal{F} (2D^2 u^4 + \mathcal{H} (2C^2 u^4 + T_0^2 v^2 + T_0^2 v^2 \cos 2\theta (\mathcal{H} - 1) + T_0^2 v^2 \mathcal{H})) \right. \\ &\quad \left. - 2u^4 v^2 \mathcal{H} (D \cos \theta + C \sin \theta)^2 \right]. \end{aligned} \quad (15)$$

Since $e^{-\phi}$ is positive, the right hand side of (14) must be positive everywhere. Then we require

$$\mathcal{B}(u) = \frac{v^2 (\mathcal{H}(u) \cos^2 \theta + \sin^2 \theta)}{\mathcal{F}(u)}, \quad (16)$$

at $u = u_c$ where the denominator $I(u)$ vanish, which implies that the integral constants satisfy

$$D = C \mathcal{H}(u) \cot \theta, \quad (17)$$

at $u = u_c$. So the determinant of induced metric can be simplified as

$$-ge^\phi = \frac{T_0^2 \mathcal{B} (-\mathcal{B} \mathcal{F} + v^2 (\cos^2 \theta \mathcal{H} + \sin^2 \theta))}{-T_0^2 u^4 \mathcal{B} \mathcal{F} + C^2 u^8 (1 + \cot^2 \theta \mathcal{H})}, \quad (18)$$

with the choices of

$$C = \pm \frac{T_0 v \sin \theta}{u_c^2}, \quad D = \pm \frac{T_0 \mathcal{H}(u_c) v \cos \theta}{u_c^2}. \quad (19)$$

Consequently, the drag forces along the x -direction and z -direction on string are given by

$$F_x = \frac{T_0 v \sin \theta}{u_c^2}, \quad F_z = \frac{T_0 \mathcal{H}(u_c) v \cos \theta}{u_c^2} \quad (20)$$

Now we consider the high-temperature solution (3). Plugging the (3) into (16), it is easy to obtain u_c to order of a^2 :

$$u_c = u_0 + u_1 a^2, \quad (21)$$

with

$$\begin{aligned}
u_0 &= \left(u_H^2 \sqrt{1-v^2} - \frac{u_H^2(-1+v^2+\sqrt{1-v^2})}{2} q^2 \right)^{1/2}, \\
u_1 &= \frac{u_H^3 \left(1 - \sqrt{1-v^2} - 5 \log 2 + 5 \log(1 + \sqrt{1-v^2}) - v^2(1 - 5 \log 2 + (4 + 3 \cos^2 \theta) \log(1 + \sqrt{1-v^2})) \right)}{48(1-v^2)^{3/4}} \\
&+ \frac{u_H^3}{384(1-v^2)^{5/4}(1+\sqrt{1-v^2})} \left(10(1-v^2)(8(1+\sqrt{1-v^2}) \log 2 - v^2(8\sqrt{1-v^2} + (8-7\sqrt{1-v^2}) \log 2)) \right. \\
&+ (-80(1+\sqrt{1-v^2}) + v^4(-86+13\sqrt{1-v^2}) + 2v^2(83+38\sqrt{1-v^2})) \log(1+\sqrt{1-v^2}) \\
&\left. + 9v^2 \cos 2\theta(2(v^2-1)(1+\sqrt{1-v^2}) + (v^2(-2+\sqrt{1-v^2}) + 2(1+\sqrt{1-v^2})) \log(1+\sqrt{1-v^2})) \right) q^2.
\end{aligned} \tag{22}$$

So, by use of (6) and (20), we can get the drag force

$$\begin{aligned}
F_x &= \frac{\pi\sqrt{\lambda}T^2v}{2} \left(\sqrt{\frac{1}{1-v^2}} - \frac{q^2}{2} \left(1 - \frac{3}{\sqrt{1-v^2}} \right) \right) + \frac{v\sqrt{\lambda}a^2}{48\pi} \left(\frac{1-v^2+\sqrt{1-v^2}+(4v^2-5)\log(1+\sqrt{1-v^2})}{(1-v^2)^{3/2}} \right. \\
&+ \frac{q^2}{2(1-v^2)^2(1+\sqrt{1-v^2})} \left(-(1+\sqrt{1-v^2})(13+30\log 2) + v^2(23+29\sqrt{1-v^2}) \right. \\
&+ 15(4+\sqrt{1-v^2})\log 2 + v^4(15\sqrt{1-v^2}\log 2 - 2(5+8\sqrt{1-v^2})+15\log 2) \\
&\left. \left. + (20(1+\sqrt{1-v^2}) + v^4(17+5\sqrt{1-v^2}) - v^2(37+22\sqrt{1-v^2})) \log(1+\sqrt{1-v^2}) \right) \right), \\
F_z &= \frac{\pi\sqrt{\lambda}T^2v}{2} \left(\sqrt{\frac{1}{1-v^2}} - \frac{q^2}{2} \left(1 - \frac{3}{\sqrt{1-v^2}} \right) \right) + \frac{v\sqrt{\lambda}a^2}{48\pi} \left(\frac{1-v^2+\sqrt{1-v^2}+(1+v^2)\log(1+\sqrt{1-v^2})}{(1-v^2)^{3/2}} \right. \\
&+ \frac{q^2}{2(v^2-1)^2(1+\sqrt{1-v^2})} \left(v^4(-1-7\sqrt{1-v^2}) - 15(2-\sqrt{1-v^2})\log 2 \right) \\
&+ v^2(2(-2+\sqrt{1-v^2}) + 15(4+\sqrt{1-v^2})\log 2) - 5(1+\sqrt{1-v^2})(-1+6\log 2) \\
&\left. - (v^2(1+v^2)(-2+\sqrt{1-v^2}) + 4(1+\sqrt{1-v^2})) \log(1+\sqrt{1-v^2}) \right),
\end{aligned} \tag{23}$$

where we have used $\theta = \pi/2$ and $\theta = 0$ which correspond to x - direction and z - direction respectively and reinstated the factor $T_0 = \frac{\sqrt{\lambda}}{2\pi}$. Note that the first part of right hand side of (23) is isotropic force in the charged plasma F_{iso} :

$$F_{iso}^q(q) = \frac{\pi\sqrt{\lambda}T^2v}{2} \left(\sqrt{\frac{1}{1-v^2}} - \frac{q^2}{2} \left(1 - \frac{3}{\sqrt{1-v^2}} \right) \right). \tag{24}$$

We can see from (24) that, in the isotropic case, the drag force in charged plasma is always larger than in neutral plasma at the same temperature. However, for anisotropic case, we will find that it will be dependent on the explicit value of q and a , which can be seen in the numerical analysis.

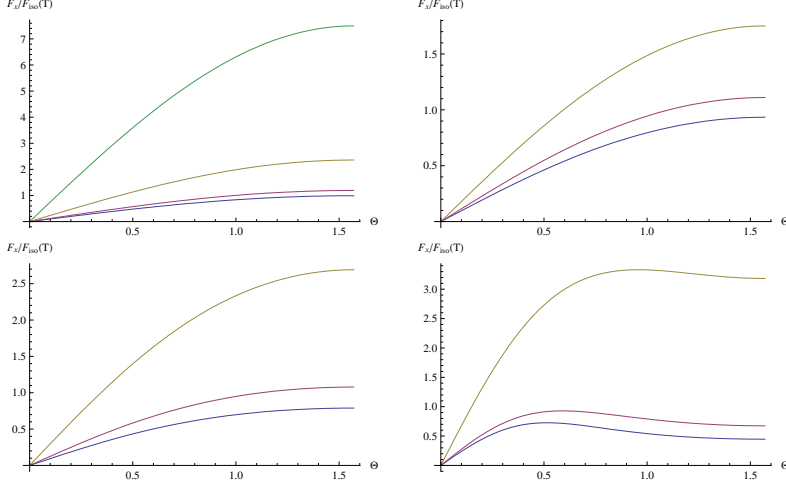


Figure 2: Drag force in x -direction F_x as a function θ at $v = 0.5$. The four graphs denote $a/T = 1.38, 4.41, 12.2, 86$ respectively, where the color lines denote $Q = 5$ (Green), $Q = 2$ (Brown), $Q = 1$ (Red), $Q = 0$ (Blue).

4 Numerical analysis

4.1 Prolate analysis

In charged anisotropic plasma, the angle dependence of drag force in x -direction in units of the isotropic drag force are shown in Fig.2 and Fig.3. From the first three plots of Fig.2¹, we can see that F_x are monotonically increasing functions of θ when $a \sim T^2$. However, the last plot of Fig.2 illustrates that F_x is no longer a monotonically increasing function of θ when $a \gg T$. By contrast, Fig.3 shows that the F_x at $v = 0.9$ is no longer a monotonically increasing function of θ when $a/T = 12.2$. We also find that for charged plasma, with fixed v , F_x can be larger than the drag force in the isotropic neutral plasma $F_{iso} \equiv F_{iso}^q (q = 0)$ for some interval of θ which depend on Q and a/T , by contrast, F_x is always smaller than F_{iso} for chargeless anisotropic plasma. Similarly, we can also plot the angle dependence of drag force in z -direction in Fig.4 and Fig.5, while F_z is always the monotonically decreasing function of θ .

The Fig.6 and Fig.7 illustrate the θ dependence of the drag force F in units of the isotropic drag force at fixed v and a/T . It is easy to see that F_x is monotonically decreasing

¹We set $u_h = 1$ in all figures.

²We also expect the same situation happens as $a \ll T$ although we do not show it here.

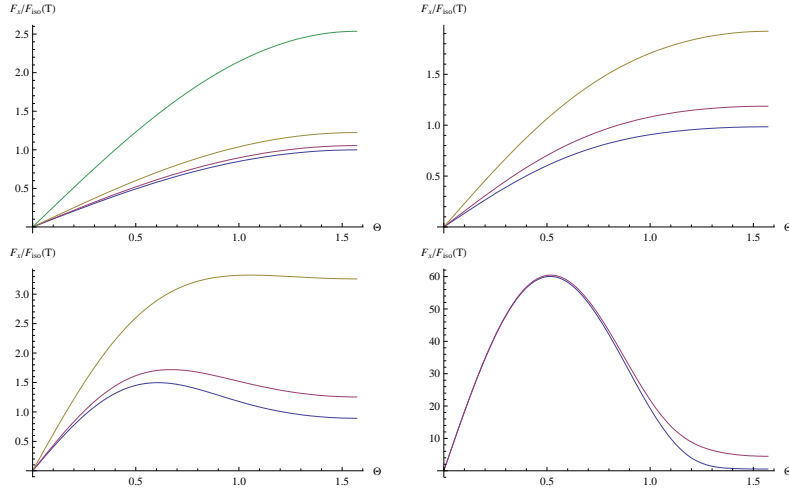


Figure 3: (color online) Drag force in x -direction F_x as a function θ at $v = 0.9$. The four graphs denote $a/T = 1.38, 4.41, 12.2, 86$ respectively. where the color lines denote $Q = 5$ (Green), $Q = 2$ (Brown), $Q = 1$ (Red), $Q = 0$ (Blue).

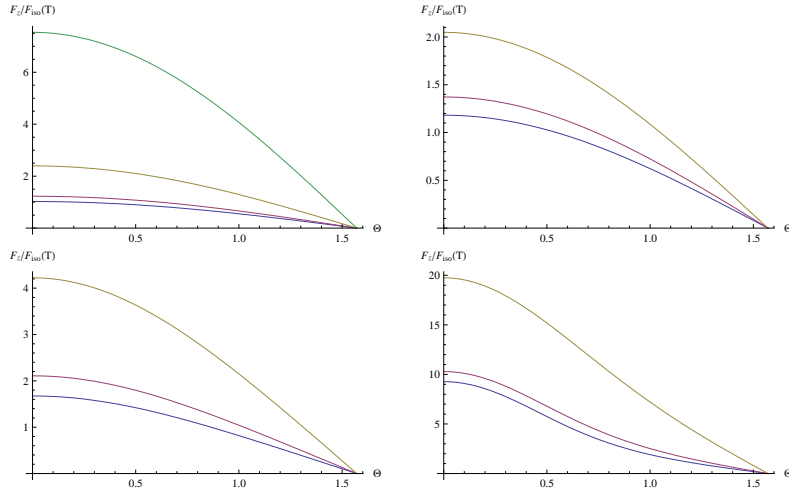


Figure 4: Drag force in z -direction F_z as a function θ at $v = 0.5$. The four graphs denote $a/T = 1.38, 4.41, 12.2, 86$ respectively, where the color lines denote $Q = 5$ (Green), $Q = 2$ (Brown), $Q = 1$ (Red), $Q = 0$ (Blue).

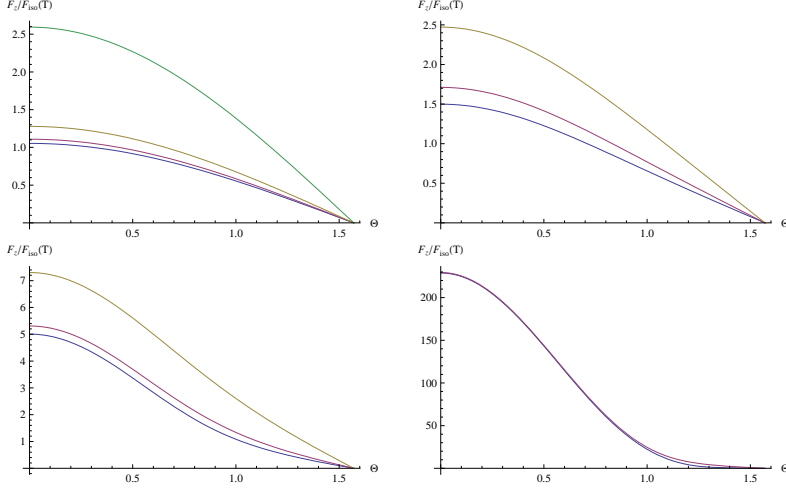


Figure 5: Drag force in z -direction F_z as a function θ at $v = 0.9$. The four graphs denote $a/T = 1.38, 4.41, 12.2, 86$ respectively, where the colour lines denote $Q = 5$ (Green), $Q = 2$ (Brown), $Q = 1$ (Red), $Q = 0$ (Blue).

functions of θ , and when a/T is greater, the falloff of F is faster.

In Fig.8-Fig.11, we can see that the drag force F in units of the isotropic drag force diverges in the ultra-relativistic limit $v \rightarrow 1$ for any $\theta \neq \pi/2$. We can see that F in charged plasma diverges faster than in chargeless plasma. So the anisotropic drag force is arbitrarily larger than the isotropic case in the ultra-relativistic limit. More interestingly, in the large Q limit, the behavior of drag force F becomes identical for different angle θ .

To exhibit the temperature-dependence of drag force more explicitly, we plot the drag force as function of a/T with different Q in Fig.12 and Fig.13. We can see that, unlike anisotropic neutral plasma, in which the drag force in the transverse direction F_x ($\theta = \pi/2$) is monotonically decreasing function of a/T , F_x in anisotropic charged plasma is the monotonically increasing function in the region with $a \ll T$ and monotonically decreasing function in the region with $a \gg T$. However, as shown in the plot of the F_z ($\theta = 0$) in Fig.13, the drag force along the longitudinal direction is always the monotonically increasing function for both neutral plasma and charged plasma.

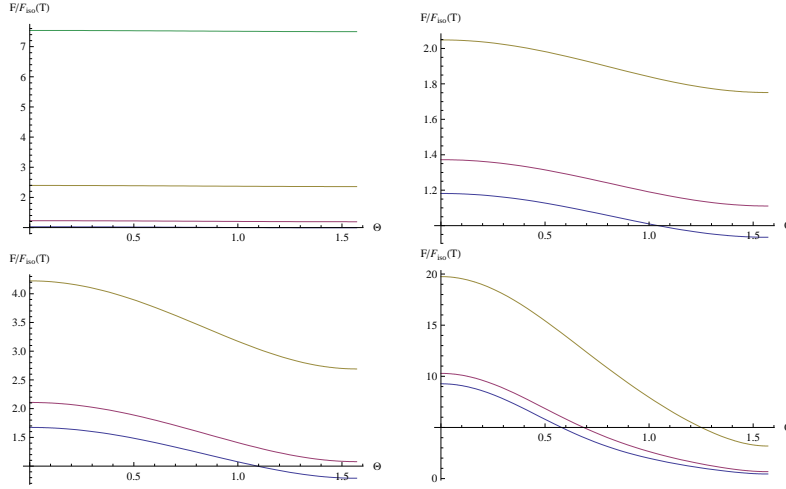


Figure 6: Drag force F as a function θ at $v = 0.5$. The four graphs denote $a/T = 1.38, 4.41, 12.2, 86$ respectively, where the color lines denote $Q = 5$ (Green), $Q = 2$ (Brown), $Q = 1$ (Red), $Q = 0$ (Blue).

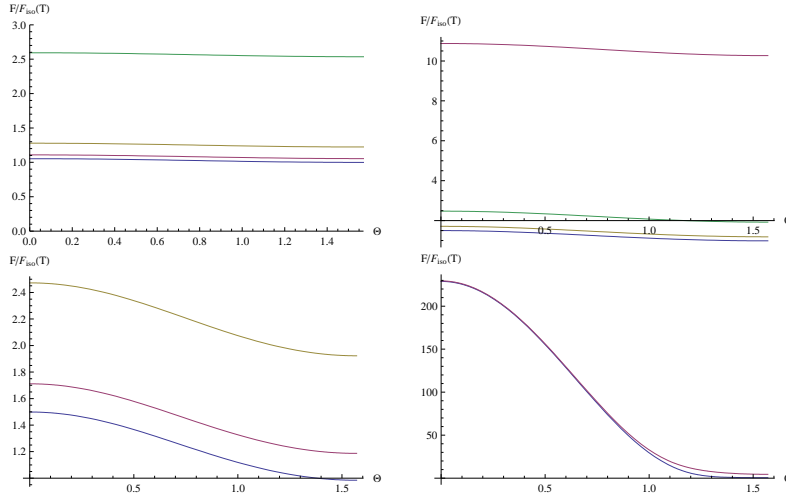


Figure 7: (color online) Drag force F as a function θ at $v = 0.9$. The four graphs denote $a/T = 1.38, 4.41, 12.2, 86$ respectively, where the color lines denote $Q = 5$ (Green), $Q = 2$ (Brown), $Q = 1$ (Red), $Q = 0$ (Blue).

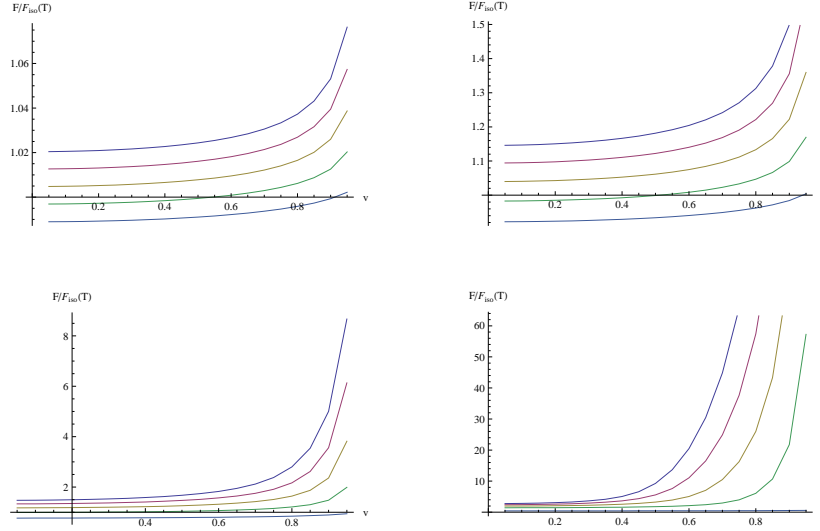


Figure 8: The drag force F as a function of velocity for a quark moving through the plasma with $Q = 0$ (i.e. chargeless). The four graphs correspond to $a/T = 1.38, 4.41, 12.2, 86$ respectively, in which five lines denote (from the top to down) $\theta = 0, \theta = \pi/6, \theta = \pi/4, \theta = \pi/3, \theta = \pi/2$.

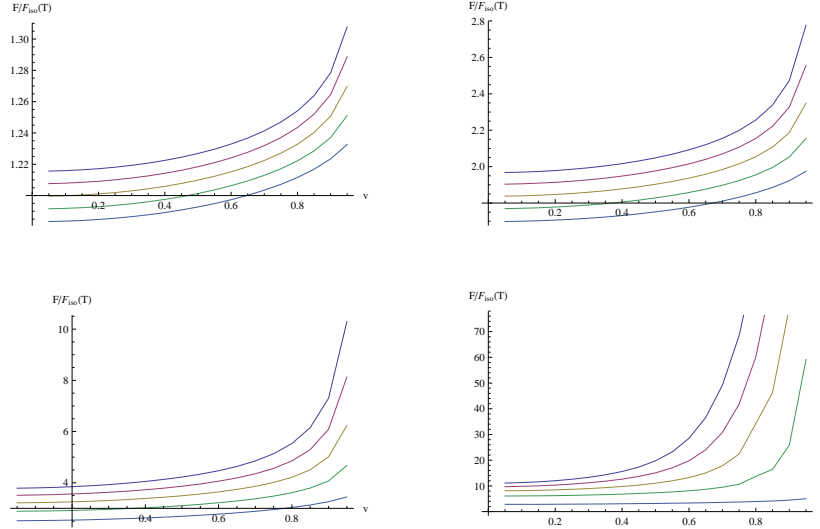


Figure 9: The drag force F as a function of velocity for a quark moving through the plasma with $Q = 2$. The four graphs correspond to $a/T = 1.38, 4.41, 12.2, 86$ respectively, in which five lines denote (from the top to down) $\theta = 0, \theta = \pi/6, \theta = \pi/4, \theta = \pi/3, \theta = \pi/2$.

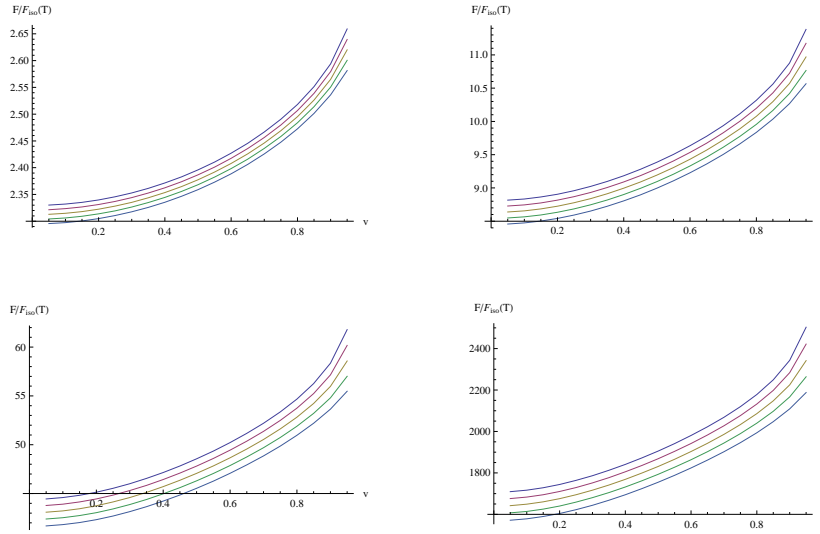


Figure 10: The drag force F as a function of velocity for a quark moving through the plasma with $Q = 5$. The four graphs correspond to $a/T = 1.38, 4.41, 12.2, 86$ respectively, in which five lines denote (from the top to down) $\theta = 0, \theta = \pi/6, \theta = \pi/4, \theta = \pi/3, \theta = \pi/2$.

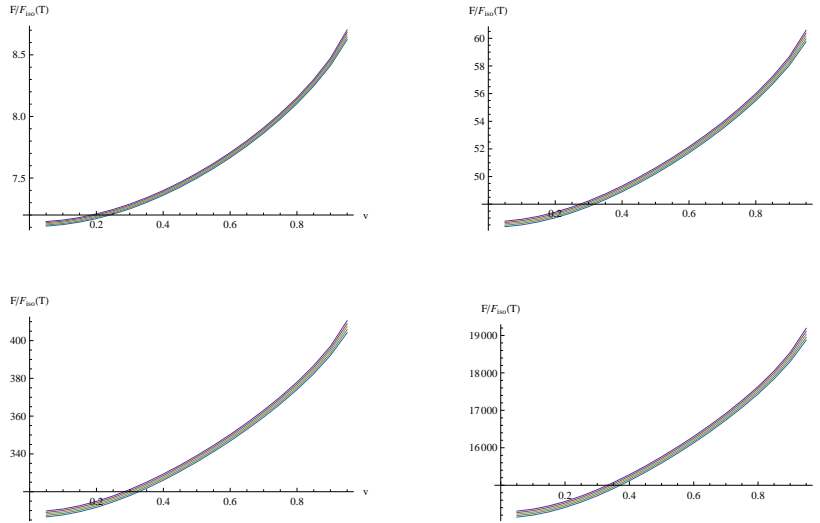


Figure 11: The drag force F as a function of velocity for a quark moving through the plasma with $Q = 10$. The four graphs correspond to $a/T = 1.38, 4.41, 12.2, 86$ respectively, in which five lines denote (from the top to down) $\theta = 0, \theta = \pi/6, \theta = \pi/4, \theta = \pi/3, \theta = \pi/2$.

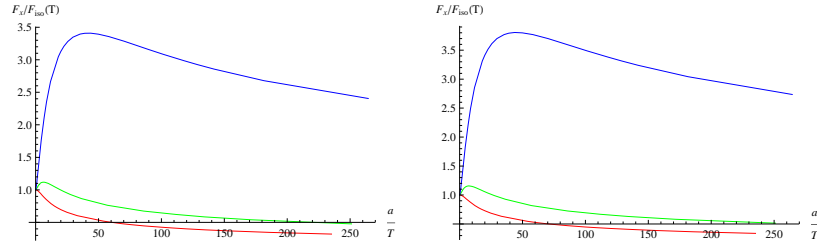


Figure 12: Drag force in x direction as a function a/T at $v = 0.5$ (left) and $v = 0.7$ (right), where the Red, Green, Blue lines represent $Q = 0, Q = 1, Q = 2$ respectively.

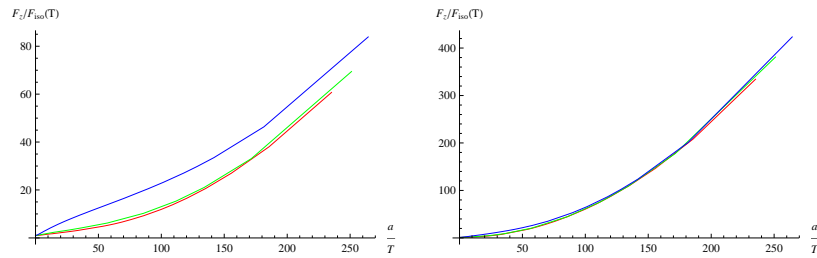


Figure 13: Drag force in z direction as a function a/T at $v = 0.5$ (left) and $v = 0.7$ (right), where the Red, Green, Blue lines represent $Q = 0, Q = 1, Q = 2$ respectively.

4.2 Oblate analysis

For oblate black brane background with $a^2 < 0$, we can also calculate the drag force. The strategy used here is similar to the one used in prolate case except that a is taken to be imaginary value here. In Fig.14, we show the θ dependence of drag force in units of the isotropic drag force. Apparently, F/F_{iso} increases as θ increases at fixed temperature and velocity which is opposite to the prolate solution. Also, as the charge Q increases, the increment of drag force from $\theta = 0$ to $\theta = \frac{\pi}{2}$ approaches to zero which is also opposite to the prolate solution where the charge Q will enhance the decrement of drag force at any angles. In Fig.15, for small charge Q , the drag force F is a monotonically decreasing function of v as v increases. However, as the charge Q increases, the drag force F becomes increasing (but not monotonically) as v increases. This indicates that there is a competing relation between the anisotropy and the charge.

The phase structure of prolate and oblate black branes are quite different. The free energy of prolate black brane has similar behavior to the AdS-Schwarzschild black hole [29]. There is a minimum temperature below which the prolate black brane is not thermodynamically favored but the oblate black brane is always thermodynamically favored for all temperature. Moreover, the oblate black brane solution yields very different thermodynamical properties compared with the prolate black brane [29], it means

$$\begin{aligned} \text{oblate : } & a^2 < 0, \quad s < s^0, \quad \Omega > \Omega^0, \quad P_z > P^0 \equiv P_{x,y}, \quad \mu > \mu^0, \\ \text{prolate : } & a^2 > 0, \quad s > s^0, \quad \Omega < \Omega^0, \quad P_z < P^0 \equiv P_{x,y}, \quad \mu < \mu^0, \end{aligned}$$

where we have not included the contribution of the renormalization scheme dependent parameter, and s^0, Ω^0, P^0 and μ^0 denote the entropy density, thermodynamical potential, pressure and chemical potential of the isotropic RN-AdS black brane. Therefore, it is not surprising that one find different behavior of drag force for the oblate anisotropy compared with the prolate case.

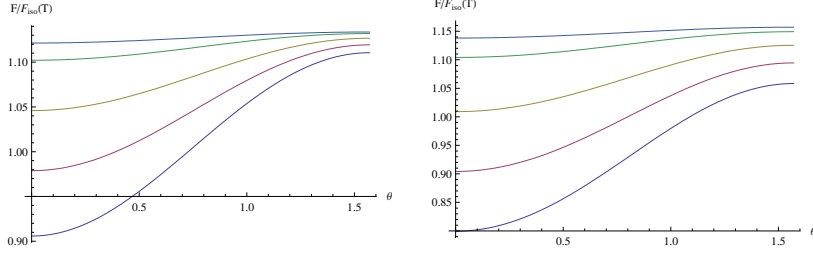


Figure 14: Drag force F of oblate solution at $T = 0.3$ as a function of θ , $v = 0.5$ (left), $v = 0.9$ (right) in which the four lines denote $Q = 0.5, Q = 1, Q = 2, Q = 5, Q = 10$ from the bottom to top.

5 Summary

By using AdS/CFT correspondence we have performed the calculations of drag force exerted on a massive quark moving through a charged, anisotropic $\mathcal{N} = 4$ SU(N) Super Yang-Mills plasma. We used the anisotropic charged black brane solution, which is dual to anisotropic QGP with a U(1) chemical potential. For a complete study of the drag force in the anisotropic background, we carried out analytic calculation first and obtain some general expressions for the drag force. Different from the isotropic case, where the drag force in charged plasma is always larger than in neutral plasma at the same temperature, for our anisotropic case, we will find that it will be dependent on the explicit value of q and a , which can be seen in the numerical analysis. For arbitrary anisotropy and charge, we presented the numerical results for any prolate and oblate anisotropy and arbitrary direction of the quark velocity with respect to the direction of anisotropy.

For prolate solution, we find the drag force in the transverse plane always increases, but decreases in the longitudinal direction with respect to the anisotropy. The decrement of drag force in the longitudinal direction is larger than the increment in the transverse direction, thus the total drag force decreases. And the effect of anisotropy and chemical potential will strengthen the increment/decrement of drag force in the transverse/longitudinal direction. On the other hand, it is surprisingly, in the large charge density limit, the velocity dependence of the drag force for different angles become identical. For the oblate solution, the transverse drag force still increases, and the longitudinal one decreases. But the total drag force increases in this case, and the increment decreases as the chemical potential increases. Furthermore, from the velocity dependence, we find there seems a competing

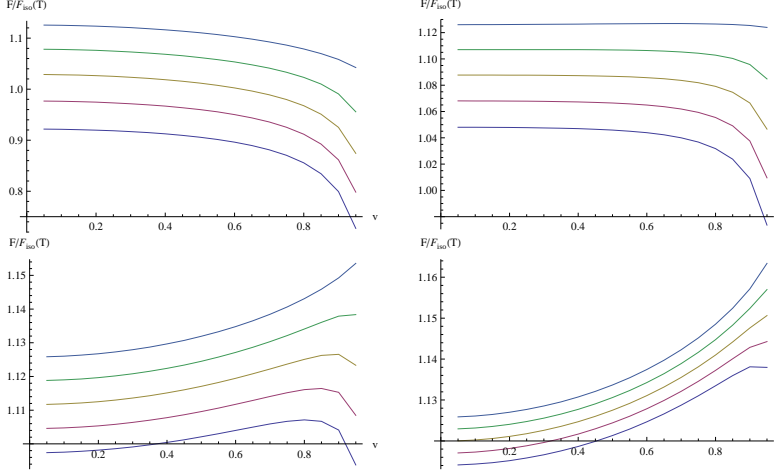


Figure 15: Drag force F of oblate solution at $T = 0.3$ as a function velocity of v . The four graphs correspond to $Q = 0.5, 2, 5, 10$ respectively, in which the five lines denote $\theta = 0, \pi/6, \pi/4, \pi/3, \pi/2$ from the bottom to top.

relation between the anisotropy and charge density for the oblate solution. We expect the opposite behavior of the oblate drag force to the prolate one might be due to the difference of their thermodynamical properties.

Finally, although we find some interesting behavior for the drag force in the oblate solution, we should emphasize that the physical meaning of oblate solution is not so clear because the imaginary value of anisotropy. So it would be interesting to understand more on the dual theory of the oblate solution. Besides, it is also interesting to consider the energy loss or jet quenching parameter in this anisotropic charged plasma. Another interesting issue to study is the photon production in this anisotropic charged plasma. This is because in this charged background the pressure along the direction of anisotropy is smaller than the transverse one which is similar to the phenomena observed in the heavy ion collision experiments. Therefore, it would be very interesting to study the production of direct photons in this background following the line of [18].

Acknowledgments

XHG was partly supported by NSFC, China (No.11375110). SYW was supported by Ministry of Science and Technology and the National Center of Theoretical Science in Taiwan

References

- [1] STAR Collaboration J. Adams *et al.*, Experimental and theoretical challenges in the search for the quark gluon plasma: The STAR collaboration’s critical assessment of the evidence from RHIC collisions, Nucl. Phys. A **757** (2005) 102 [nucl-ex/0501009].
- [2] PHENIX Collaboration ,K. Adcox *et al.*, Formation of dense partonic matter in relativistic nucleus collisions at RHIC: Experimental evaluation by the PHENIX collaboration, Nucl. Phys. A **757** (2005) 184 [nucl-ex/0410003].
- [3] J. M. Maldacena, The Large N limit of superconformal field theories and supergravity, Adv. Theor. Math. Phys. **2** (1998) 231 [hep-th/9711200].
- [4] S. S. Gubser, I. R. Klebanov, A. M. Polyakov, Gauge theory correlators from noncritical string theory, Phys. Lett. **B428** (1998) 105 [hep-th/9802109].
- [5] E. Witten, Anti-de Sitter space and holography, Adv. Theor. Math. Phys. **2** (1998) 253 [hep-th/9802150].
- [6] S.A.Hartnoll, Lectures on holographic methods for condensed matter physics; arXiv:0903.3246
- [7] John McGreevy, Holographic duality with a view toward many-body physics, arXiv:0909.0518
- [8] S. A. Hartnoll, C. P. Herzog and G. T. Horowitz, “Building a Holographic Superconductor,” Phys. Rev. Lett. **101**, 031601 (2008) [arXiv:0803.3295 [hep-th]].
- [9] W. Y. Wen, M. S. Wu and S. Y. Wu, “A Holographic Model of Two-Band Superconductor,” Phys. Rev. D **89**, 066005 (2014) [arXiv:1309.0488 [hep-th]].
- [10] X. H. Ge, B. Wang, S. F. Wu and G. H. Yang, “Analytical study on holographic superconductors in external magnetic field ,” JHEP 1008, 108(2010) [arXiv:1002.4901 [hep-th]].
- [11] S. Kachru, X. Liu and M. Mulligan, “Gravity duals of Lifshitz-like fixed points,” Phys. Rev. D **78**, 106005 (2008) [arXiv:0808.1725 [hep-th]].
- [12] J. R. Sun, S. Y. Wu and H. Q. Zhang, “Novel Features of the Transport Coefficients in Lifshitz Black Branes,” Phys. Rev. D **87**, 086005 (2013) [arXiv:1302.5309 [hep-th]].

- [13] J. R. Sun, S. Y. Wu and H. Q. Zhang, “Mimic the optical conductivity in disordered solids via gauge/gravity duality,” *Phys. Lett. B* **729**, 177 (2014) [arXiv:1306.1517 [hep-th]].
- [14] L. Q. Fang, X. H. Ge and X. M. Kuang, “ Holographic fermions in charged Lifshitz theory,” *Phys.Rev. D* **86** 105037 (2012) [arXiv:1201.3832 [hep-th]]
- [15] J. Casalderrey-Solana, H. Liu, D. Mateos, K. Rajagopal, U. A. Wiedemann, Gauge/String Duality, Hot QCD and Heavy Ion Collisions, arXiv:1101.0618.
- [16] Youngman Kim, Ik Jae Shin, Takuya Tsukioka Holographic QCD: Past, Present, and Future, arXiv:1205.4852.
- [17] S. Caron-Huot, P. Kovtun, G. D. Moore, A. Starinets and L. G. Yaffe, “Photon and dilepton production in supersymmetric Yang-Mills plasma,” *JHEP* **0612**, 015 (2006) [hep-th/0607237].
- [18] S. Y. Wu and D. L. Yang, “Holographic Photon Production with Magnetic Field in Anisotropic Plasmas,” *JHEP* **1308**, 032 (2013) [arXiv:1305.5509 [hep-th]].
- [19] B. Muller, S. Y. Wu and D. L. Yang, “Elliptic flow from thermal photons with magnetic field in holography,” *Phys. Rev. D* **89**, no. 2, 026013 (2014) [arXiv:1308.6568 [hep-th]].
- [20] G. Policastro, D. T. Son and A. O. Starinets, The shear viscosity of strongly coupled $N = 4$ supersymmetric Yang-Mills plasma, *Phys. Rev. Lett.* **87** (2001) 081601 [hep-th/0104066].
- [21] C. P. Herzog, A. Karch, P. Kovtun, C. Kozcaz, L. G. Yaffe, Energy loss of a heavy quark moving through $N=4$ supersymmetric Yang-Mills plasma, *JHEP* **0607** (2006) 013, [hep-ph/0605158]
- [22] Steven S. Gubser, Drag force in AdS/CFT, *Phys. Rev. D* **74**, 126005, [hep-ph/0605182]
- [23] Sang-Jin Sin, Ismail Zahed, Holography of Radiation and Jet Quenching, *Phys.Lett. B* **608** (2005) 265, [hep-th/0407215].
- [24] Hong Liu, Krishna Rajagopal, Urs Achim Wiedemann, Calculating the Jet Quenching Parameter from AdS/CFT, *Phys. Rev. Lett.* **97**, 182301, [hep-ph/0605178]

- [25] H. U. Yee, “Holographic Chiral Magnetic Conductivity,” JHEP **0911**, 085 (2009) [arXiv:0908.4189 [hep-th]].
- [26] D. E. Kharzeev and H. U. Yee, “Chiral Magnetic Wave,” Phys. Rev. D **83**, 085007 (2011) [arXiv:1012.6026 [hep-th]].
- [27] S. Pu, S. Y. Wu and D. L. Yang, “Holographic Chiral Electric Separation Effect,” Phys. Rev. D **89**, 085024 (2014) [arXiv:1401.6972 [hep-th]].
- [28] S. Pu, S. Y. Wu and D. L. Yang, “Chiral Hall Effect and Chiral Electric Waves,” arXiv:1407.3168 [hep-th].
- [29] L. Cheng, X. H. Ge, S.J. Sin, Anisotropic plasma with a chemical and schemen-independent instablities, Phys. Lett. B 734 (2014) 116 [arXiv:1404.1994]
- [30] L. Cheng, X.H. Ge and S. J. Sin, Anisotropic plasma at finite $U(1)$ chemical potential, JHEP 07 (2014) 083 [arXiv:1404.5027]
- [31] D. Mateos and D. Trancanelli, Thermodynamics and instabilities of a strongly coupled anisotropic plasma, JHEP 1107 (2011) 054 [arXiv:1106.1637].
- [32] D. Mateos and D. Trancanelli, The anisotropic $N=4$ super Yang-Mills plasma and its instabilities , Phys. Rev. Lett. 107 (2011) 101601 [arXiv:1105.3472].
- [33] M. Chernicoff, D. Fernandez, D. Mateos and Diego Trancanelli, Drag force in a strongly coupled anisotropic plasma, JHEP 1208 (2012) 100 [arXiv:1202.3696].
- [34] D. Giataganas, Probing strongly coupled anisotropic plasma, JHEP **1207**,(2012) 031 [arXiv:1202.4436].
- [35] M. Chernicoff, D. Fernandez, D. Mateos and Diego Trancanelli, Jet quenching in a strongly coupled anisotropic plasma, JHEP 1208 (2012) 041 [arXiv:1203.0561].
- [36] B. Muller and D. L. Yang, “Light Probes in a Strongly Coupled Anisotropic Plasma,” Phys. Rev. D **87**, no. 4, 046004 (2013) [arXiv:1210.2095 [hep-th]].
- [37] S. Chakraborty and N. Haque, “Drag force in strongly coupled, anisotropic plasma at finite chemical potential,” arXiv:1410.7040 [hep-th].